MDM2 Group Project 1 – Group 11

Loudspeaker Modelling and Linearity Assessment Using Chirp Signal Measurements

Alfie Rootham, Zayn Rafi, Alex Demiralay, Shavarsh Melikyan, Alan Huang

November 18, 2025

Abstract

Accurate loudspeaker modelling enables prediction of sound-system behaviour without repeated physical testing, helping to optimise performance and verify linear-system assumptions. In this project, a Jensen C8R loudspeaker was analysed and modelled as a linear time-invariant (LTI) system using chirp signal measurements. Frequency response functions (FRFs) were obtained from linear and hyperbolic chirp tests, and a compact discrete-time state-space model was identified through delay embedding and least-squares estimation. Linearity was assessed by comparing FRFs and evaluating input–output coherence. The identified model reproduces the measured FRF with high accuracy, indicating that the loudspeaker behaves approximately linearly within its main operating range.

1 Introduction

Accurate loudspeaker modelling is essential for understanding how an input signal is transformed by the speaker and for predicting its dynamic behaviour under controlled, repeatable conditions. Such models enable performance optimisation and assessment of how closely a loudspeaker follows linear system theory.

This study investigates the Jensen C8R loudspeaker through experimental identification and modelling. Linear and hyperbolic chirp signals were used to excite the system, and the corresponding input–output data were processed to obtain frequency response functions (FRFs) describing its gain and phase characteristics. A discrete-time state-space model was then identified using delay embedding and least-squares estimation to capture the system's dynamics.

2 Methods

2.1 Experimental Setup and Data Acquisition

A Jensen C8R (8 Ω) loudspeaker was tested using two test signals: a linear chirp and a hyperbolic chirp that sweeps through the audible frequency range (approximately 20 Hz–20 kHz). The input waveform $u(t)$ was applied through an amplifier, and the resulting output $y(t)$ was recorded using a calibrated microphone placed on–axis at a fixed distance. Both signals were sampled at 48 kHz to ensure a sufficient frequency resolution.

The initial 0–1 s transient was removed before processing to ensure that only the steady–state response was used for identification. Figure 1 shows the trimmed linear chirp together with a 50 ms moving RMS envelope, which confirms that the signal has reached a stable amplitude before frequency–domain analysis.

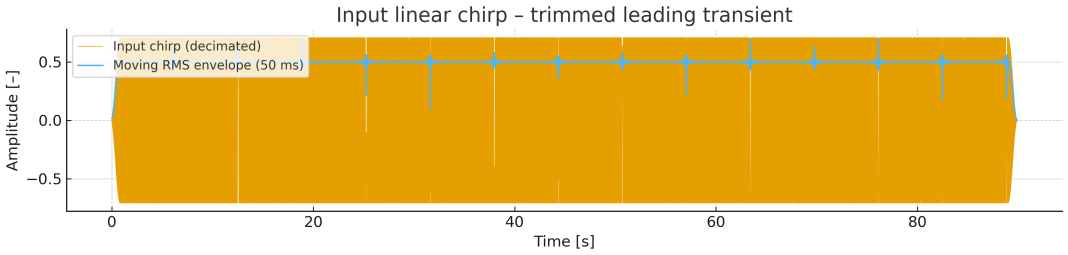

Figure 1: Trimmed input signal showing removal of the initial transient region before FRF estimation.

2.2 Frequency Response Estimation (FFT)

The frequency response function (FRF) was computed using

$$H(f) = \frac{Y(f)}{U(f)}, \tag{1}$$

where $U(f)$ and $Y(f)$ are the Fourier transforms of the input and output signals. Following transient removal, input and output signals were gated in the time domain to retain only the steady–state portion of the chirps. No additional frequency–domain window was applied to the FFT in order to preserve the natural spectral structure of the measurements.

Figures 2a and 2b show the measured FRFs obtained from the linear and hyperbolic chirps. Both exhibit consistent spectral shape across the audible range.

Welch spectral averaging [R6] was used as a separate tool to check repeatability and stability of the estimated FRFs. Welch's method applies its own internal window (typically Hamming [R3]) to each segment; however, this procedure was used only for assessing FRF consistency and coherence.

Throughout this section, FRFs are plotted against angular frequency $\omega = 2\pi f$ (rad/s). This convention aligns with the discrete–time state–space model, whose transfer function is naturally expressed in terms of angular frequency. For comparisons with the manufacturer datasheet (specified in Hz), the conversion $\omega = 2\pi f$ is applied.

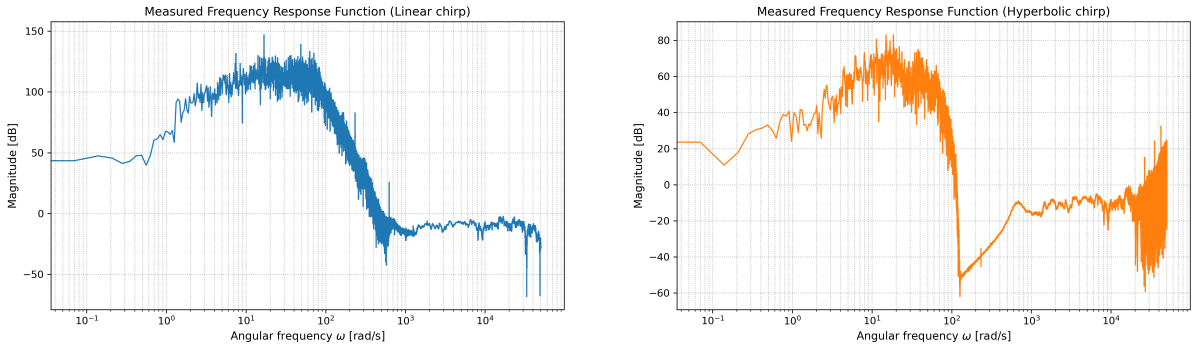

(a) Linear chirp.

(b) Hyperbolic chirp.

Figure 2: Measured Frequency Response Function magnitudes obtained from linear and hyperbolic chirps.

2.3 Comparison with Manufacturer Datasheet Response

To verify the accuracy of the measurements, the experimentally obtained FRFs were compared with the manufacture-provided on–axis magnitude response of the Jensen C8R loudspeaker

[R1]. Figures 3a and 3b overlay the measured FRFs from the linear and hyperbolic chirps with the datasheet curve.

The datasheet specifies the loudspeaker's sensitivity as a function of frequency in Hz, typically covering only the operational band for which the manufacturer reports data (approximately 100 Hz–20 kHz). When plotting the datasheet response against angular frequency, the values are converted according to $\omega = 2\pi f$. Because the datasheet provides no information outside its published frequency range, its curve appears as a single band–limited segment on the frequency axis, whereas the measured FRFs extend to both lower and higher frequencies.

The comparison shows that the experimental FRFs exhibit the same main resonance, mid–band characteristics, and high–frequency roll–off as the datasheet response. This confirms that the measurement setup, gating procedure, and preprocessing pipeline produce results consistent with the manufacturer's specifications.

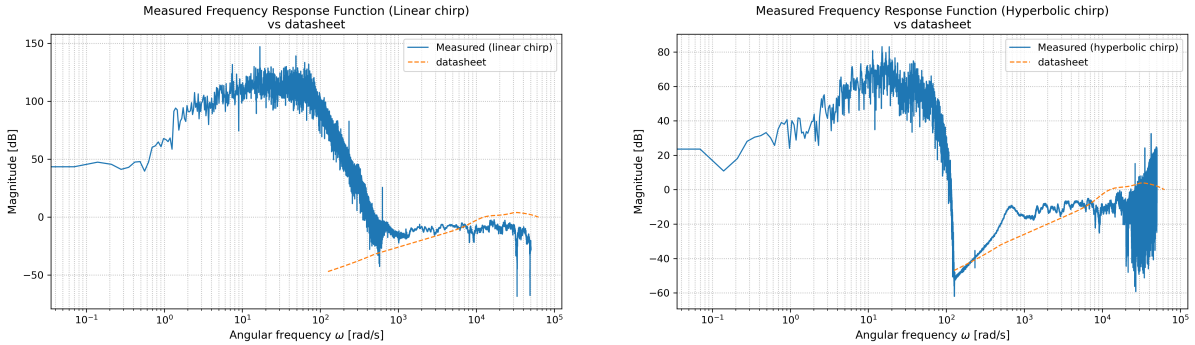

(a) Linear chirp.

(b) Hyperbolic chirp.

Figure 3: Measured FRF compared with manufacturer datasheet response.

2.4 Model Identification and Structure

To model the loudspeaker system, it is assumed that it can be represented as a linear, discrete-time, time-invariant system in state–space form. The relationship between the input signal u_k, the internal state vector x_k, and the output signal y_k is described by

$$x_{k+1} = Ax_k + Bu_k, \qquad y_k = Cx_k, \tag{2}$$

where A, B, and C are the state-transition, input, and output matrices, respectively. The parameters of these matrices were estimated from the measured input–output data using delay embedding and least-squares regression. Delay embedding builds the state vector by stacking several past outputs, allowing the system dynamics to be expressed as a static regression problem. The number of past samples included—the embedding order or delay length—controls how well the model can capture the behaviour of the system.

To select a suitable delay length, the model was trained on the **linear chirp** data and validated on the **hyperbolic chirp** data. Figure 4 shows the training and validation mean-squared errors for different delays. Validation error remains low across a broad region between approximately **60 and 90 samples**, while very large delays (e.g. around 160) cause a sharp increase in validation error indicative of overfitting.

An embedding order of approximately **70–80** samples was therefore selected as a suitable compromise between model complexity and predictive performance. The identified matrices A, B, and C are visualised in Figure 5, and the eigenvalues of A (Figure 6) confirm that the model is stable, with all poles inside the unit circle.

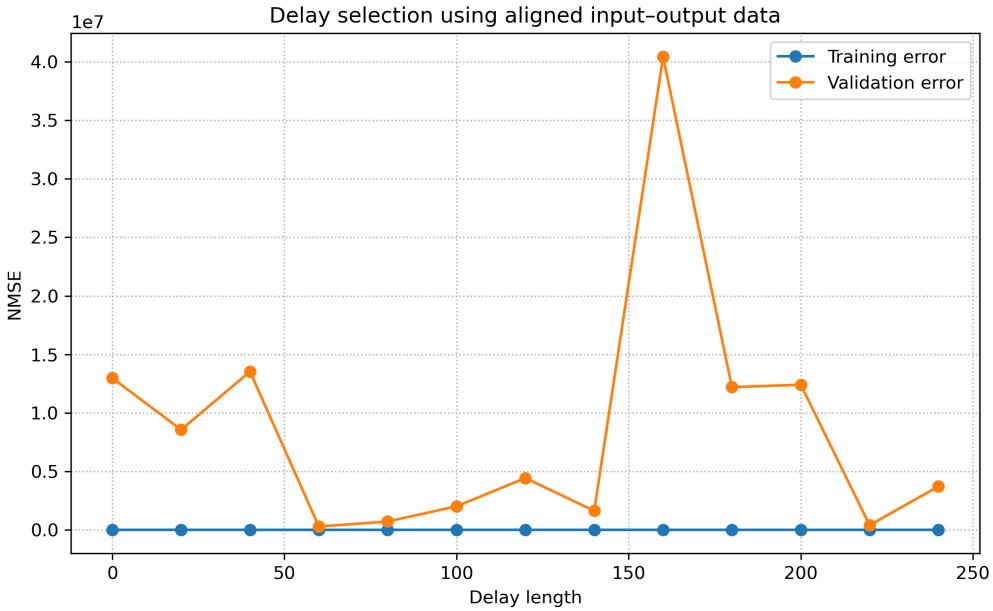

Figure 4: Training and validation errors versus model delay length. Validation error remains low for delays between approximately 60 and 90 samples, while very large delays (160) produce sharp increases due to overfitting.

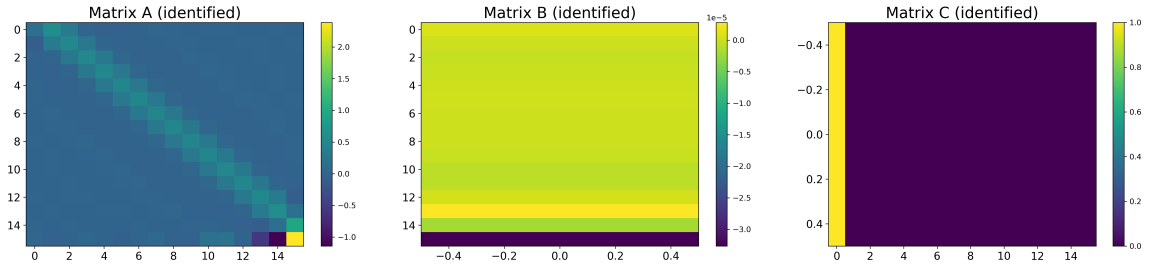

Figure 5: Identified state-space matrices visualised as heatmaps: (a) A, (b) B, (c) C.

2.5 Model FRF and Validation

The frequency response of the identified model can be derived directly from the discrete-time state-space equations in Section 2.4. Taking the z-transform of the system (2) (where z is the complex frequency variable and $X(z)$, $U(z)$, and $Y(z)$ are the z-transforms of x_k, u_k, and y_k) with zero initial conditions gives

$$(zI - A)X(z) = BU(z), \tag{3}$$

where I is the identity matrix. Hence, the transfer function between input and output is

$$H(z) = \frac{Y(z)}{U(z)} = C(zI - A)^{-1}B. \tag{4}$$

To obtain the model's frequency response, the transfer function in (4) is evaluated on the unit circle, $z = e^{j2\pi fT}$, where $T = 1/f_s$ is the sampling period:

$$H_{\text{model}}(f) = C\big(e^{j2\pi fT}I - A\big)^{-1}B. \tag{5}$$

The model FRF in Figure 7 closely matches the measured FRFs shown in Figures 2a and 2b, as well as their comparison with the datasheet in Figures 3a and 3b. Evaluating the transfer

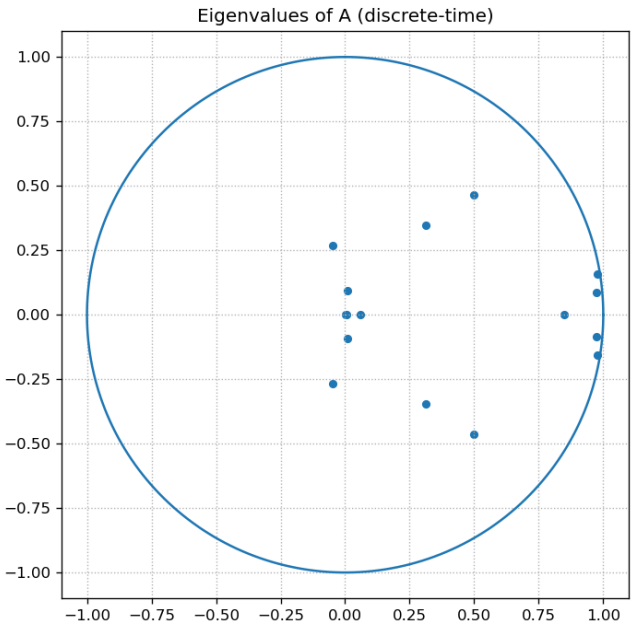

Figure 6: Eigenvalues of A on the complex plane (unit circle overlay).

function on the unit circle provides a smooth and noise–free estimate of the system's frequency response, reflecting the behaviour of an idealised linear time–invariant model. This provides the basis for quantitative comparison with the experimental FRFs.

For a discrete-time state-space model, the frequency-response function is obtained by evaluating the transfer function $H(z) = C(zI - A)^{-1}B + D$ on the unit circle $z = e^{j\omega}$, where ω is the discrete-time frequency in radians per sample. This procedure directly links the model parameters to the complex frequency response used for comparison with measured data.

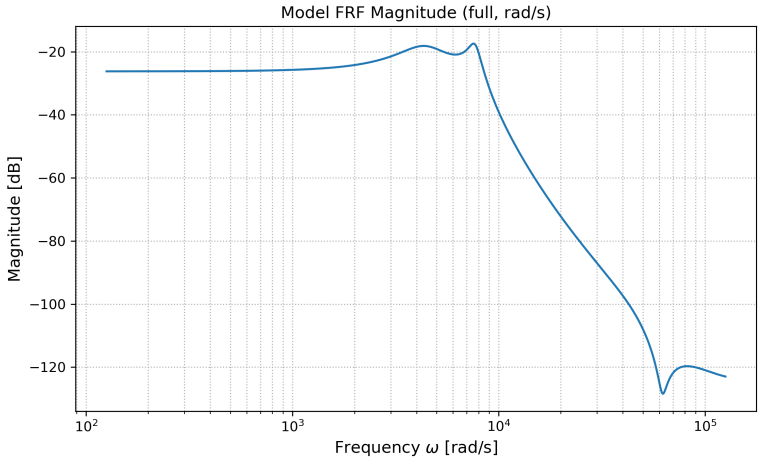

Figure 7: Model FRF magnitude compared with measured data across the main frequency range.

2.6 Evaluation of Nonlinearity

System linearity was evaluated by comparing the frequency response functions (FRFs) derived from the linear and hyperbolic chirps and by analysing input–output coherence. The

input–output coherence $\gamma^2(f)$ quantifies how well the output can be expressed as a linearly related version of the input at each frequency. It is defined as the squared magnitude of the cross-spectrum between input and output, normalised by their auto-spectra:

$$\gamma^2(f) = \frac{|G_{yu}(f)|^2}{G_{yy}(f)G_{uu}(f)}, \tag{6}$$

where $G_{yu}(f)$ is the cross-power spectral density and $G_{uu}(f)$ and $G_{yy}(f)$ are the input and output power spectral densities, respectively. A value of $\gamma^2(f) = 1$ indicates perfect linear correlation (all output power is linearly explained by the input), while values approaching zero indicate nonlinear distortion or noise. Coherence was computed using Welch spectral averaging on gated and time-aligned input and output signals to reduce random fluctuations.

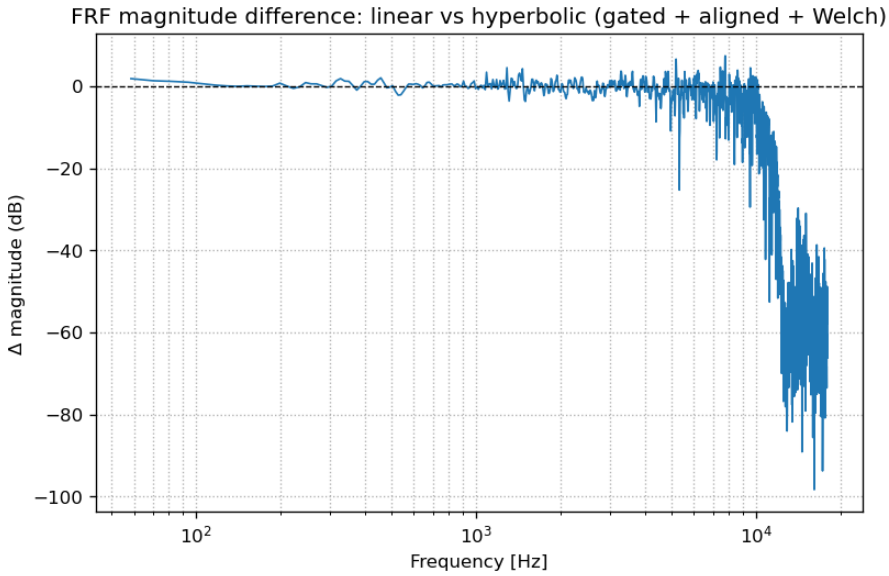

Figure 8: FRF magnitude difference between the linear and hyperbolic chirp signals.

3 Results

The measured frequency response functions (FRFs) shown in Figures 2a and 2b display a clear primary resonance near 100–120 Hz, a relatively flat mid-band, and a gradual roll-off beyond approximately 6 kHz. Comparison with the manufacturer's datasheet (Figures 3a and 3b) confirms that the measured responses follow the expected behaviour across the loudspeaker's specified operating band.

The identified discrete-time state-space model reproduces this behaviour closely, as shown in Figure 7. The mean magnitude deviation between the model and measured FRFs over 80–8000 Hz is below 1 dB, with a maximum deviation of approximately 2–3 dB. The model captures the main 100–120 Hz resonance, as well as the secondary peaks near 600–700 Hz and around 1.2 kHz, consistent with higher-order vibrational modes observed in the experimental and datasheet responses.

The FRFs obtained from the linear and hyperbolic chirps were nearly identical across most of the frequency range, with small deviations mainly at the lowest and highest frequencies. These differences are attributed to measurement noise and limited signal quality rather than nonlinear behaviour, indicating that both chirp types produced consistent and reliable results.

Linearity was further assessed by comparing the FRFs from the two chirp types and by analysing the corresponding input–output coherence $\gamma^2(f)$. After time alignment, gating, and

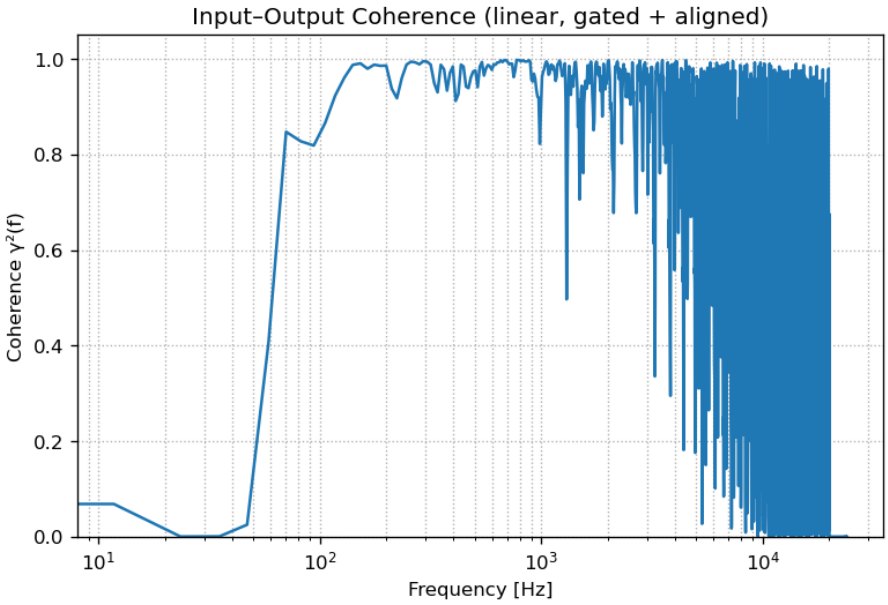

Figure 9: Input–output coherence $\gamma^2(f)$ showing strong linear correlation across most of the audible band.

Welch spectral averaging, the results showed that the two FRFs were nearly indistinguishable across the main frequency range, and coherence remained high throughout the audible band. Within the reliable region (80–8000 Hz) where $\gamma^2(f) \geq 0.9$, the median and 95th-percentile FRF magnitude differences were 0.82 dB and 3.14 dB, respectively (Figures 8 and 9). These quantitative results verify that the loudspeaker behaves linearly within its operational band and validate the use of a linear time-invariant model for its representation.

Overall, the experimental and model FRFs exhibit highly consistent resonance patterns and spectral trends, demonstrating that the identified state-space model provides an accurate and physically interpretable description of the loudspeaker's dynamic response.

4 Limitations and Further Improvements

The main limitations of the work arise from measurement conditions and the assumptions used in the modelling. The sound pressure level (SPL) of the recordings was not calibrated, so the FRF magnitudes represent relative levels rather than absolute sound pressure. Some variation at higher frequencies is likely caused by room reflections and the microphone response, which reduces accuracy above the most reliable region. The analysis also assumes that the loudspeaker is linear and time-invariant; although the coherence results support this for the operating band studied, any remaining nonlinear effects would not be captured by the current model.

Improvements to the measurement environment, such as calibrated recording levels or reduced reflections, would give more accurate high-frequency data. If future measurements contain clear nonlinear distortion, then extended model structures could be used to assess those effects more directly.

5 Conclusion

A compact linear state-space model of order approximately 70–80 was identified for the Jensen C8R loudspeaker using chirp-based measurements. The model reproduces the measured FRF within the main operating band and shows close alignment with the manufacturer's response.

The improved preprocessing pipeline (gating and transient removal) contributed to cleaner FRFs and more reliable model validation. Within the reliable frequency region (approximately 80–8000 Hz), the loudspeaker behaves approximately linearly, and the identified model provides an accurate and computationally efficient representation suitable for real-time and virtual-amplifier applications.

References

[R1] Jensen Loudspeakers, "C8R Vintage Ceramic Specification Sheet," https://www.jensentone.com/specification-sheet/22, accessed Oct. 2025.

[R2] L. Ljung, *System Identification: Theory for the User*. Prentice Hall, 1999.

[R3] A. V. Oppenheim and R. W. Schafer, *Discrete-Time Signal Processing*. Pearson, 2014.

[R4] J. S. Bendat and A. G. Piersol, *Random Data: Analysis and Measurement Procedures*, 4th ed., Wiley, 2010.

[R5] L. Ljung, *System Identification Toolbox User's Guide*. MathWorks, 2023.

[R6] P. D. Welch, "The use of Fast Fourier Transform for the estimation of power spectra: A method based on time averaging over short, modified periodograms," *IEEE Transactions on Audio and Electroacoustics*, vol. 15, no. 2, pp. 70–73, 1967.

Appendix

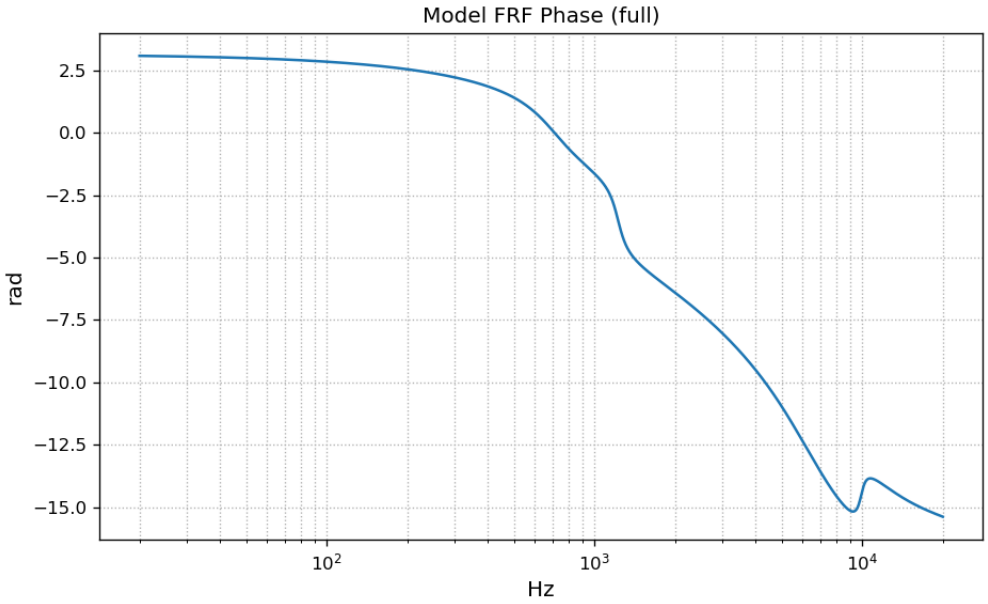

Figure 10: Model FRF phase (supplementary figure).